Electrolyte Gate-Controlled Kondo Effect in $SrTiO_3$

Menyoung Lee,[1] J. R. Williams,[1] Sipei Zhang,[2] C. Daniel Frisbie,[2] and D. Goldhaber-Gordon[1,*]

[1]*Department of Physics, Stanford University, Stanford, California 94305, USA*

[2]*Department of Chemical Engineering and Materials Science, University of Minnesota, Minneapolis, Minnesota 55455, USA*

(Received 5 August 2011; published 12 December 2011)

We report low-temperature, high-field magnetotransport measurements of $SrTiO_3$ gated by an ionic gel electrolyte. A saturating resistance upturn and negative magnetoresistance that signal the emergence of the Kondo effect appear for higher applied gate voltages. This observation, enabled by the wide tunability of the ionic gel-applied electric field, promotes the interpretation of the electric field-effect-induced 2D electron system in $SrTiO_3$ as an admixture of magnetic Ti^{3+} ions, i.e., localized and unpaired electrons, and delocalized electrons that partially fill the Ti 3*d* conduction band.

DOI: 10.1103/PhysRevLett.107.256601 PACS numbers: 72.15.Qm, 72.15.Gd, 75.20.Hr, 75.47.Lx

The Coulomb interaction amongst electrons and ions in a solid can spontaneously generate internal magnetic fields and effective magnetic interactions. Unexpected magnetic phenomena may emerge whenever we consider a new system where interactions are important. In recent years, predictions for and observations of magnetism originating in the two-dimensional (2D) system of electrons at the interface between $SrTiO_3$ (STO) and $LaAlO_3$ (LAO) have attracted much attention [1–7], particularly the prediction of charge disproportionation and the emergence of +3-valent Ti sites with unpaired spin [1] and direct measurements of in-plane magnetization [6,7]. The conducting electrons at the LAO/STO interface are believed to be induced by polar LAO's strong internal electric fields, and to reside on the Ti sites on the STO side of the interface, partially filling the lowest-lying Ti 3*d* bands [8–10]. Questions remain, however, over the role of the growth process, in particular, whether oxygen vacancy formation or cation intermixing are in fact responsible for the observed *n*-type conduction [11–14].

Other than growing a polar overlayer, a 2D system of electrons in STO can be made by chemical doping with Nb, La, or oxygen vacancies [15–18], or purely electrostatic charging in an electric double layer transistor (EDLT) [19,20]. If electronic reconstruction in response to overlayer polarity is an accurate description for LAO/STO, then that system can be closely modeled by field-effect-induced electrons in undoped STO, where confounding questions over growth conditions do not arise, and the applied electric field can be widely tuned.

In this Letter, we expand on the body of evidence for Ti^{3+} magnetism in STO that conducts in two dimensions. We demonstrate a gate-controlled Kondo effect in the 2D electron system in undoped STO formed beneath the bare surface by the electric field from an ionic gel electrolyte, and interpret this system as an admixture of magnetic Ti^{3+} ions (unpaired and localized electrons) and delocalized electrons partially filling the Ti 3*d* conduction band, as predicted theoretically [2,21]. The Kondo effect is an archetype for the emergent magnetic interactions amongst localized and delocalized electrons in conducting alloys [22,23], and the ability to produce and tune the effect by purely electrostatic means in any conducting system is of interest in its own right [24,25]. The observed appearance of the Kondo effect in STO as a function of an applied electric field points to the emergence of magnetic interactions between electrons in STO due to electron-electron correlations rather than the presence of dopants.

We report measurements from two STO Hall bar devices (*A* and *B*), gated using an ionic gel electrolyte in an EDLT configuration. Behaviors similar to those we show have been observed in 6 devices. A schematic showing the operation of the devices is shown in Fig. 1(a), and a

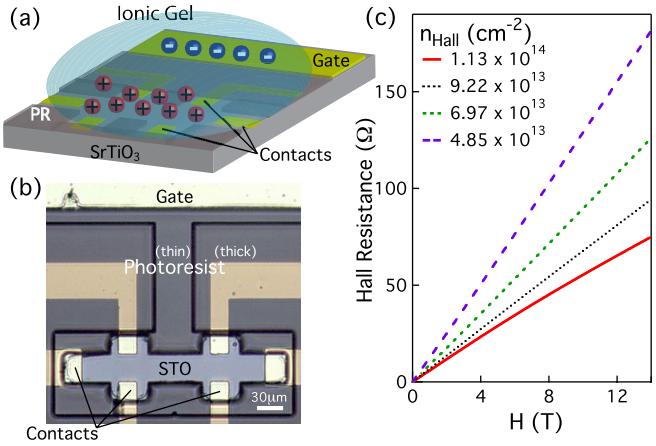

FIG. 1 (color online). (a) Schematic diagram of the EDLT operation. PR = photoresist. (b) Optical micrograph of a device identical to those measured. The photoresist (dark regions) is partially transparent, and contact leads can be seen through it. The "thin" region of the photoresist has a thickness of 1 μm, while the "thick" region has 2 μm. (c) Hall resistance of device *A* at $T = 5$ K, to measure the accumulated electron density on the STO surface channel. $V_g = +3.5$ V for the highest density, and subsequent lower densities were set by allowing the electrolyte to partially lose polarization at $T \approx 200$ K.

photograph of a device identical to those we measured but without the electrolyte is shown in Fig. 1(b). Undoped STO (100) crystals (MTI Corp.) were treated with buffered hydrofluoric acid to obtain a TiO_2-terminated surface [26], and the crystal for device B was then annealed at 1000 °C in a tube furnace with 50 sccm of flowing oxygen gas. The Hall bar geometry, 30 μm wide and 100 μm long between the voltage leads, was defined via a window through a 1 μm-thick film of hard-baked photoresist that exposes the channel and the gate to the electrolyte while keeping the rest of the STO separated from the ions and hence still insulating. Prior to the lithographic definition of the Hall bar, contacts were created by Ar^+ ion milling to a dose of 2 C/cm^2 with 300 V acceleration [27] then depositing Al/Ti/Au electrodes with thickness of 40/5/100 nm. The ionic gel electrolyte was formed by the gelation of a triblock copolymer poly(styrene-*block*-methylmethacrylate-*block*-styrene) (PS-PMMA-PS) in an ionic liquid 1-ethyl-3-methylimidazolium bis(trifluoromethanesulfonyl) amide (EMI-TFSA, formerly referred to as EMI-TFSI) [28,29]. A drop of gel was formed on another substrate, then manually pasted over the device, covering both the STO channel and the 200 μm $\times$ 400 μm coplanar metal gate.

The magnetotransport characteristics of device A were measured in a Physical Property Measurement System (Quantum Design) at temperatures down to $T = 4.5$ K and magnetic fields up to $H = 14$ T. The sample was insulating at the start and the end of the experiment, indicating that the conduction was not due to doping by electrochemical reactions. At room temperature, the gate voltage was ramped up to $V_g = +3.5$ V, which polarized the electrolyte, pushing cations toward the channel. The electric field of the ions caused the accumulation of electrons that form our 2D system in STO. Then the sample was cooled to $T = 5$ K, during which the leakage current through the gate dropped below the measurement limit of 100 pA for $T < 200$ K, signaling the freezing of EMI-TFSA. Once at $T = 5$ K, V_g was nulled and magnetotransport measurements were taken. To apply a weaker electric field and set the electron density lower, the device was warmed to $T \approx 200$ K, and the electrolyte was allowed to partially lose its polarization, decreasing the accumulated cation concentration at the channel and correspondingly the electron density in the STO.

We measured the longitudinal resistance R of the device as a function of temperature and an applied magnetic field, using standard lock-in techniques at quasi-DC frequencies <100 Hz with a current bias <5 nA and no additional source-drain bias. Figure 1(c) shows Hall resistance measurements at $T = 5$ K, which show that the electron density inferred from the Hall effect decreases for each successive cooldown, from $n_{\mathrm{Hall}} = 1.13 \times 10^{14}$ cm^{-2} in the first cooldown, to $n_{\mathrm{Hall}} = 4.85 \times 10^{13}$ cm^{-2} for the last. We have measured densities as high as 7×10^{14} cm^{-2} in some other samples, but the devices described here with $n_{\mathrm{Hall}} \sim 10^{13}$ to 10^{14} cm^{-2} showed lower disorder and have the observed density and other transport features most similar to other high-mobility 2D systems in STO.

The 2D nature of our samples is evident from three magnetoresistance features, which have not been reported in previous EDLT studies of STO: the dependence of the Hall resistance as a function of $H_\perp = H\cos\theta$, weak antilocalization, and Shubnikov–de Haas oscillations (see Supplementary Material [30]). Weak antilocalization, with similarly strong spin-orbit coupling strengths, has been reported in the LAO/STO interface and attributed to the Rashba-type coupling due to inversion asymmetry of the interface [31]. Shubnikov–de Haas oscillations were seen in device B at $V_g = +2.8$ V, which gave $n_{\mathrm{Hall}} = 2.6 \times 10^{13}$ cm^{-2}. The electron density inferred from the oscillation period was much lower at 3×10^{12} cm^{-2} if only a twofold spin degeneracy is assumed (see Supplementary Material [30]). Reported quantum oscillations of the magnetoresistance in LAO/STO and δ-doped STO have yielded similarly low values of the inferred electron density [15,17,32,33].

The magnetoresistance of the sample, $R(H) - R(H = 0)$, measured at the highest electron density, is plotted in Fig. 2(a) for various directions of $\vec{H}$. When $\vec{H}$ is normal to the sample plane ($\theta = 0$), the magnetoresistance is positive, and as the $\vec{H}$ direction is tilted away from normal and into the sample plane, the magnetoresistance crosses over from positive to negative at $\theta \approx 75°$. A similar crossover from positive out-of-plane magnetoresistance to negative in-plane magnetoresistance has been reported in LAO/STO [34].

We pay particular attention to the sample's zero-field resistance as a function of temperature, $R(T)$. Figure 2(b)

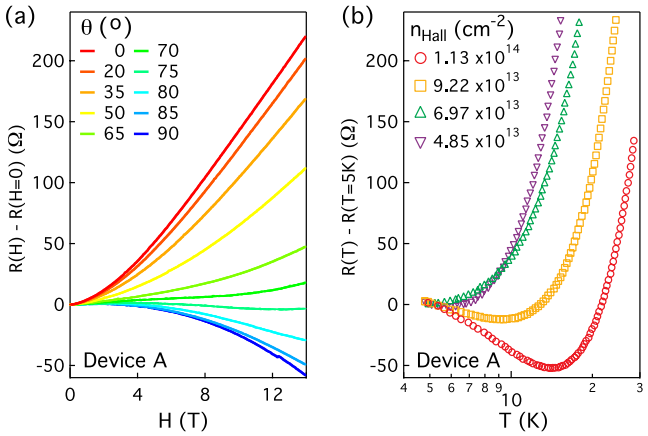

FIG. 2 (color online). (a) Device A magnetoresistance for various directions of $\vec{H}$ at the highest electron density, where $n_{\mathrm{Hall}} = 1.13 \times 10^{14}$ cm^{-2}. Angle θ is measured from the normal to sample plane, and $\theta = 90°$ is $\vec{H} \parallel \vec{j}$. $T = 5$ K. (b) Device A $R(T) - R(T = 5\ \mathrm{K})$ for each measured density in $H = 0$, showing the observed $R(T)$ upturn strengthen for higher density.

shows the resistance relative to its value at $T = 5$ K, $R(T) - R(T = 5\ \mathrm{K})$, at each measured electron density. At the highest density, a minimum is seen at $T = 14$ K and the resistance turns upward, and this upturn is substantially weakened as the density is lowered. The appearance of a resistance minimum and low-temperature upturn, unexpected for a metallic system, at higher electron density suggests that the electric field-induced electrons, not added impurities, are themselves responsible for the scattering, and electron-electron correlations strongly influence the transport properties. A disorder-induced metal-insulator transition, by contrast, ought to show a stronger upturn at lower density, not the opposite trend seen here. The precise threshold density for the emergence of an $R(T)$ minimum differs amongst samples, but the overall trend is the same. Reducing the induced 2D electron density reduces the low-temperature upturn in resistance.

To further investigate these anomalies we measured device B at lower temperatures down to 1.4 K and higher magnetic fields up to 31 T. We set $V_g = +3.5$ V for the first cooldown and measured $n_{\mathrm{Hall}} = 5.3 \times 10^{13}\ \mathrm{cm}^{-2}$ at $T = 1.4$ K. To set lower densities for subsequent cooldowns, we set lower $V_g = +3.2$, 2.8, and 2.2 V at $T \approx 200$ K then waited for ~15 minutes for the electrolyte to equilibrate, rather than nulling V_g and quickly obtaining a partial loss of polarization as described above for device A.

Figure 3 shows the device B zero-field $R(T)$ at $V_g = +3.5$ V, corresponding to the highest electron density measured in this sample. A minimum of $R(T)$ is seen at $T = 14.5$ K, and then the upturn saturates at the lowest temperatures, such that $d^2R/dT^2 < 0$ for $T < 7$ K. This saturating resistance upturn is suppressed in subsequent cooldowns at lower gate voltages, and thus the same overall trend in the behavior of $R(T)$ with respect to electron density is observed in both devices. Finally, in the last cooldown and lowest density, a nonsaturating upturn and localization-like behavior is observed (see Supplementary Material [30]).

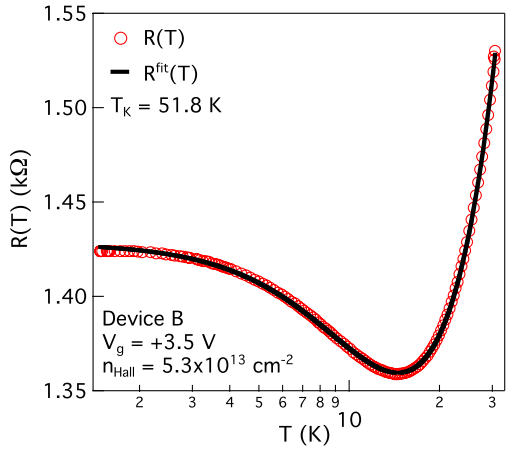

FIG. 3 (color online). Device B longitudinal resistance in $H = 0$ as a function of temperature at $V_g = +3.5$ V. The Hall effect yielded $n_{\mathrm{Hall}} = 5.3 \times 10^{13}\ \mathrm{cm}^{-2}$ at $T = 1.4$ K. Solid curve: A fit using Eqs. (1) and (2). $R_0 = 607\ \Omega$, $q = 0.437\ \Omega/\mathrm{K}^2$, $p = 1.2 \times 10^{-8}\ \Omega/\mathrm{K}^5$, $R_K(0\ \mathrm{K}) = 819\ \Omega$, and $T_K = 51.8$ K.

The appearance of a saturating resistance upturn at low temperature is characteristic of the Kondo effect, where the temperature dependence of the contribution from magnetic impurities to the electrical resistivity of a metal is a universal function in units of a single temperature scale, the Kondo temperature T_K. This universal function $R_K(T/T_K)$ behaves logarithmically at high temperature $T \gg T_K$, and saturates at low-temperature, so that $R_K(T/T_K) \approx R_K(0\ \mathrm{K})\ (1 - 6.088(T/T_K)^2)$ for $T \ll T_K$ if we define T_K as the temperature at which the Kondo resistivity is half relative to its zero-temperature value [22,35]. Across the whole measured temperature range from 1.4 to 30 K, which includes temperatures above and below the observed $R(T)$ minimum, the resistance can be described well by a simple Kondo model

$$R^{\mathrm{fit}}(T) = R_0 + qT^2 + pT^5 + R_K(T/T_K), \qquad (1)$$

where R_0 is the residual resistance due to sample disorder, and the T^2 and T^5 terms represent the functional temperature dependences of the electron-electron and the electron-phonon interactions, respectively. For the numerical fitting of this model to the data, we used an empirical form for the universal resistivity function,

$$R_K(T/T_K) = R_K(T = 0)\left(\frac{T_K'^2}{T^2 + T_K'^2}\right)^s, \qquad (2)$$

where $T_K' = T_K/(2^{1/s} - 1)^{1/2}$, and we fixed $s = 0.225$ to closely match the theoretical result obtained by the numerical renormalization group [35,36]. A numerical fit using Eqs. (1) and (2) to the measured $R(T)$ curve yielded $R_0 = 607\ \Omega$, $q = 0.437\ \Omega/\mathrm{K}^2$, $p = 1.2 \times 10^{-8}\ \Omega/\mathrm{K}^5$, $R_K(0\ \mathrm{K}) = 819\ \Omega$, and $T_K = 51.8$ K.

Device B, with $\vec{H}$ applied parallel to the sample plane and $\vec{H} \perp \vec{j}$, also exhibited a strong negative magnetoresistance, up to $\approx -20\%$ at $H_{\parallel} = 31$ T, and its $R(H_{\parallel})$ is plotted in Fig. 4. The temperature-dependent magnetoresistance at $V_g = +3.5$ V, plotted in Fig. 4(a), shows that raising the sample temperature suppresses the negative in-plane magnetoresistance such that the effect disappears between 30 and 40 K. In the highest fields $H_{\parallel} > 25$ T, the Kondo resistance upturn is sufficiently suppressed such that resistance depends monotonically on temperature. Such a temperature dependence of the magnetoresistance is expected from the splitting of the Kondo peak in the spectral function by an applied magnetic field, which leads to negative magnetoresistance by suppressing the Kondo effect on the resistance [37,38].

Measurements of $R(H_{\parallel})$ were done at each gate voltage at the lowest temperature $T = 1.4$ K, and the results are plotted in Fig. 4(b) along with their comparison to a simple Kondo model

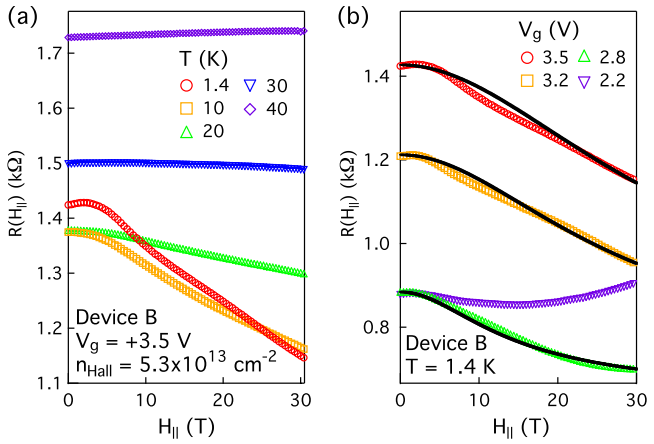

FIG. 4 (color online). (a) Device B in-plane magnetoresistance ($\vec{H} \perp \vec{j}$) at $V_g = +3.5$ V and various temperatures. The negative magnetoresistance is gradually suppressed as the temperature is raised, and the resistance increases with the temperature in the highest $H_{\|}$. (b) The same at all four applied gate voltages at $T = 1.4$ K. Solid curves: $R^{\text{model}}(H_{\|})$ according to Eq. (3) where we chose $R_0 = 607\ \Omega$ and $H_1 = 20$, 16, and 8 T for $V_g = +3.5$, 3.2, and 2.8 V, respectively.

$$R^{\text{model}}(H_{\|}) = R_0 + R_K(H_{\|}/H_1), \tag{3}$$

where now $R_K(H_{\|}/H_1)$ is the universal function for zero-temperature magnetoresistivity of a Kondo impurity, related to its magnetization which may be calculated using Bethe-ansatz techniques, and H_1 is a magnetic scale related to the Kondo temperature and the g factor of the impurity spin [39]. To compare the data and model we numerically evaluated the exact form of $R_K(H_{\|}/H_1)$ (see Supplementary Material [30] and [39]) and chose $H_1 =$ 20, 16, and 8 T to compare with the data obtained at $V_g =$ +3.5, 3.2, and 2.8 V, respectively. The comparison is not exact and fails for low fields, where weak antilocalization and other effects may be relevant, but the overall dependence and shape are broadly consistent, particularly for the lower density at $V_g = +2.8$ V. At $V_g = +3.5$ V, we note an order-of-magnitude match between the fit Kondo temperature and the magnetic energy scale; $g\mu_B H_1 \approx k_B T_K$, where equality holds to within a factor of 2 if we assume $g = 2$.

The negative in-plane magnetoresistance is suppressed at lower electron density, and so the same trend with respect to density is apparent in $R(H)$ as well as in $R(T)$ measurements. The dependence of low-temperature Kondo resistivity on changing the Fermi level, with impurity concentration held fixed, is expected to be given by $R_K(T = 0, H = 0) \propto n_e^{-1}\nu_0^{-1}$, where n_e and ν_0 are the conduction electrons' number density and density of states at the Fermi level [38]. Hence, the Kondo resistivity, due to unintentional impurities like iron, must increase when electron density is decreased. We, however, observe the opposite trend; the Kondo resistivity is suppressed at lower density. Hence, we rule out magnetic atom impurities as the cause and infer that the observed Kondo effect originates from the electrons accumulated at the surface by the applied electric field. As the Kondo effect arises due to the interaction between localized and delocalized electrons, we can interpret our observations by viewing the 2D electron system as an admixture composed of localized and unpaired electrons—perhaps polaronic in nature [2]—that act as the Kondo scattering centers and a metal of delocalized electrons that partially fill the Ti 3d conduction band.

Finally, we comment on the implications of the results described herein for the ongoing efforts to conclusively understand the LAO/STO interface, where an $R(T)$ minimum and negative magnetoresistance have already been reported [3]. By electrostatically inducing 2D electrons in STO, we have modeled the essential physics of the polar catastrophe, and the demonstration of a gate-controlled Kondo effect in undoped STO shows that the observations of electronic conduction and magnetism in LAO/STO are plausibly due to electronic reconstruction and are not necessarily a result of unintended doping during LAO growth [5,10]. By exploiting the wide gate tunability afforded by the electrolyte, we have identified the electron density on the STO surface as the critical tuning parameter connecting the variety of electronic phenomena that have been reported in LAO/STO and electrolyte-gated STO studies—from the localization of carriers and the metal-insulator transition [19,40] to the Kondo effect and magnetism [3–7]. The magnetic interactions found in STO, added to its other attractive features, including the tunability of the ground state by applied electric fields and superconductivity, show STO-based interfaces and heterostructures to be a promising playground in which to look for and study emergent electronic phenomena and novel device applications [41,42].

We thank J. Jaroszynski, S. Stemmer, B. Jalan, I. R. Fisher, J. G. Analytis, A. Falk, M. Chalfin, E. Eason, Y. Cui, J. J. Cha, Y. Lee, T. A. Costi, S. Ilani, and A. Joshua. The development of the ionic gating technique was supported as part of the Center on Nanostructuring for Efficient Energy Conversion, an Energy Frontier Research Center funded by the U.S. Department of Energy, Office of Science, Office of Basic Energy Sciences under Grant No. DE-SC0001060. The measurement and study of STO were supported by the MURI program of the Army Research Office Grant No. W911-NF-09-1-0398. The Minnesota contribution was supported by the National Science Foundation through the MRSEC program at the University of Minnesota, Grant No. DMR-0819885. M. L. is partially supported by Samsung and Stanford University. A portion of this work was performed at the National High Magnetic Field Laboratory, which is supported by National Science Foundation Cooperative Agreement No. DMR-0654118, the State of Florida, and the U.S. Department of Energy.

*goldhaber-gordon@stanford.edu

[1] R. Pentcheva and W. E. Pickett, Phys. Rev. B **74**, 035112 (2006).
[2] B. R. K. Nanda and S. Satpathy, Phys. Rev. B **83**, 195114 (2011).
[3] A. Brinkman *et al.*, Nature Mater. **6**, 493 (2007).
[4] D. A. Dikin *et al.*, Phys. Rev. Lett. **107**, 056802 (2011).
[5] M. Huijben *et al.*, Adv. Mater. **21**, 1665 (2009).
[6] L. Li *et al.*, Nature Phys. **7**, 762 (2011).
[7] J. A. Bert *et al.*, Nature Phys. **7**, 767 (2011).
[8] N. Nakagawa, H. Y. Hwang, and D. A. Muller, Nature Mater. **5**, 204 (2006).
[9] M. Salluzzo *et al.*, Phys. Rev. Lett. **102**, 166804 (2009).
[10] D. G. Schlom and J. Mannhart, Nature Mater. **10**, 168 (2011).
[11] W. Siemons *et al.*, Phys. Rev. Lett. **98**, 196802 (2007).
[12] G. Herranz *et al.*, Phys. Rev. Lett. **98**, 216803 (2007).
[13] P. Willmott *et al.*, Phys. Rev. Lett. **99**, 155502 (2007).
[14] A. Kalabukhov *et al.*, Europhys. Lett. **93**, 37001 (2011).
[15] Y. Kozuka *et al.*, Nature (London) **462**, 487 (2009).
[16] J. Son *et al.*, Nature Mater. **9**, 482 (2010).
[17] B. Jalan *et al.*, Phys. Rev. B **82**, 081103 (2010).
[18] A. F. Santander-Syro *et al.*, Nature (London) **469**, 189 (2011).
[19] K. Ueno *et al.*, Nature Mater. **7**, 855 (2008).
[20] Y. Lee *et al.*, Phys. Rev. Lett. **106**, 136809 (2011).
[21] Z. S. Popovic, S. Satpathy, and R. M. Martin, Phys. Rev. Lett. **101**, 256801 (2008).
[22] J. Kondo, Prog. Theor. Phys. **32**, 37 (1964).
[23] G. Gruner and A. Zawadowski, Rep. Prog. Phys. **37**, 1497 (1974).
[24] D. Goldhaber-Gordon *et al.*, Nature (London) **391**, 156 (1998).
[25] J.-H. Chen *et al.*, Nature Phys. **7**, 535 (2011).
[26] M. Kawasaki *et al.*, Science **266**, 1540 (1994).
[27] D. W. Reagor and V. Y. Butko, Nature Mater. **4**, 593 (2005).
[28] J. H. Cho *et al.*, Nature Mater. **7**, 900 (2008).
[29] J. Lee *et al.*, J. Phys. Chem. C **113**, 8972 (2009).
[30] See Supplemental Material at http://link.aps.org/supplemental/10.1103/PhysRevLett.107.256601 for further detailed discussion of EDLT device characteristics, electron system 2-dimensionality, and Kondo magnetoresistance.
[31] A. D. Caviglia *et al.*, Phys. Rev. Lett. **104**, 126803 (2010).
[32] A. D. Caviglia *et al.*, Phys. Rev. Lett. **105**, 236802 (2010).
[33] M. Ben Shalom *et al.*, Phys. Rev. Lett. **105**, 206401 (2010).
[34] M. Ben Shalom *et al.*, Phys. Rev. B **80**, 140403 (2009).
[35] T. A. Costi, A. C. Hewson, and V. Zlatic, J. Phys. Condens. Matter **6**, 2519 (1994).
[36] D. Goldhaber-Gordon *et al.*, Phys. Rev. Lett. **81**, 5225 (1998).
[37] W. Felsch and K. Winzer, Solid State Commun. **13**, 569 (1973).
[38] T. A. Costi, Phys. Rev. Lett. **85**, 1504 (2000).
[39] N. Andrei, K. Furuya, and J. Lowenstein, Rev. Mod. Phys. **55**, 331 (1983).
[40] S. Thiel *et al.*, Science **313**, 1942 (2006).
[41] H. Takagi and H. Y. Hwang, Science **327**, 1601 (2010).
[42] J. Mannhart and D. G. Schlom, Science **327**, 1607 (2010).